Sol-gel based synthesis and enhanced processability of MAX phase Cr2GaC

Journal:	*Journal of Materials Chemistry C*
Manuscript ID	TC-ART-03-2019-001416.R1
Article Type:	Paper
Date Submitted by the Author:	15-Apr-2019
Complete List of Authors:	Siebert, Jan Paul ; Arizona State University, School of Molecular Sciences Bischoff, Lothar; Eduard Zintl Institute of Inorganic and Physical Chemistry, Lepple, Maren; DECHEMA Forschungsinstitut, High Temperature Materials Zintler, Alexander; Technische Universität Darmstadt, Department of Material- and Earth Sciences Molina-Luna, Leopoldo; Technische Universität Darmstadt, Department of Material- and Earth Sciences Wiedwald, Ulf; University of Duisburg-Essen, Faculty of Physics Birkel, Christina; Arizona State University

SCHOLARONE™
Manuscripts

Journal Name

ARTICLE

Sol-gel based synthesis and enhanced processability of MAX phase Cr₂GaC

Jan Paul Siebert,[a,b] Lothar Bischoff,[b] Maren Lepple,[b] Alexander Zintler,[c] Leopoldo Molina-Luna,[c] Ulf Wiedwald[d,e] and Christina S. Birkel *[a,b]

MAX phases are typically prepared by high-temperature (oftentimes high-pressure) solid-state methods. Here, we report a new wet chemistry based synthesis technique starting from an aqueous solution of metal nitrates and citric acid to prepare MAX phase Cr₂GaC. This solution-processable precursor mixture has the potential to be easily scaled, painted, printed or fabricated onto supports – an advantage that is demonstrated by the formation of hollow carbon microspheres which are decorated with Cr₂GaC particles. A small amount of chromium carbide and oxide remains in the product, however, the amount of the latter can be reduced by a larger excess in citric acid in the precursor gel. The transformation mechanism of the initial amorphous gel into highly crystalline and anisotropic MAX phase particles is investigated by detailed thermal analysis. Transmission electron microscopy studies are conducted to elucidate the microstructure of the sol-gel-prepared particles as well as the decorated hollow microspheres. From magnetic susceptibility measurements, the density of states at the Fermi level is deduced reflecting the quality of the Pauli paramagnet Cr₂GaC.

Introduction

Sol-gel chemistry is widely used for the synthesis of inorganic solids and dates back to the early work on silica gels in the mid-1800s.[1] Roughly 100 years later, it stimulated significant advances in the synthesis of new compounds, such as novel ceramic oxides,[2,3] as well as the commercial development of colloidal silica powders (*Ludox*, Du Pont). The sol-gel process first involves the formation of a colloidal suspension ("sol") that is transformed into a network structure ("gel"). Already at this step, chemists can get creative by producing a number of different types of gels from varying precursors and with varying bonding types.[4,5] Condensation within the network then typically continues ("aging") prior to drying of the gel during which the porous structure usually collapses. Depending on the target compound, an annealing step is added in order to remove the M-OH surface groups and to promote crystallization of the solid. Based on this approach, sol-gel chemistry has evolved into a highly established synthesis tool for new materials. In contrast to classical solid-state techniques where diffusion is the rate-limiting step – and often unreacted precursors and undefined

morphologies occur – the biggest advantage of the sol-gel method lies in the intimate mixing of the starting materials on an atomic/molecular level. This ensures shorter diffusion paths and faster mass transport, thus lower reaction temperatures and shorter reaction times can usually be employed for the synthesis of the solid-state material. Besides, sol-gel syntheses can lead to nanostructured and metastable compounds, as has been demonstrated for different binary and ternary carbides, such as Fe₃C,[6] WC, Mo₂C, Cr₃C₂,[7] Ni₆Mo₆C.[8,9]

It is important to note that the term sol-gel chemistry has broadened significantly from its original use focusing on hydrolysis and condensation processes. The common approach therefor involves using molecular precursors in a liquid phase to synthesize a solid. The literature is rich in numerous modifications of the original sol-gel process (e.g. solution combustion synthesis) based on different starting materials, gelation agents and reaction temperatures/annealing steps.[5,10] Layered ternary carbides and nitrides that crystallize in the hexagonal space group $P6_3/mmc$, initially described as H-phases,[11] are summarized as the family of MAX phases with more than 70 members to date. They have the general composition $M_{1+n}AX_n$ (n is usually 1,2,3), where M is an early transition metal, A is a main group element, mostly of groups 13-15, and X is either carbon or nitrogen.[12,13] They have attracted considerable attention because of their unique mechanical properties,[14] interesting magnetic behavior[15] and lately as precursors for two-dimensional MXenes[16] with a plethora of possible applications.[17] Bulk MAX phases are traditionally prepared by high-temperature solid-state reactions,[13] such as arc melting and annealing,[18,19] reactive hot pressing[20,21] and self-propagating high-temperature synthesis,[22,23] starting from metals or metal hydrides.

[a.] School of Molecular Sciences, Arizona State University, Tempe, AZ-85282, USA
[b.] Eduard-Zintl-Institut für Anorganische und Physikalische Chemie, Technische Universität Darmstadt, 64287 Darmstadt, Germany.
[c.] Department of Material- and Earth Sciences, Advanced Electron Microscopy, Technische Universität Darmstadt, 64287 Darmstadt, Germany.
[d.] Faculty of Physics and Center for Nanointegration Duisburg-Essen, University of Duisburg-Essen, Germany.
[e.] National University of Science and Technology «MISIS», Moscow, Russian Federation.
Electronic Supplementary Information (ESI) available: Details on synthesis and characterization, additional XRD data, SEM images and magnetometry data. See DOI: 10.1039/x0xx00000x
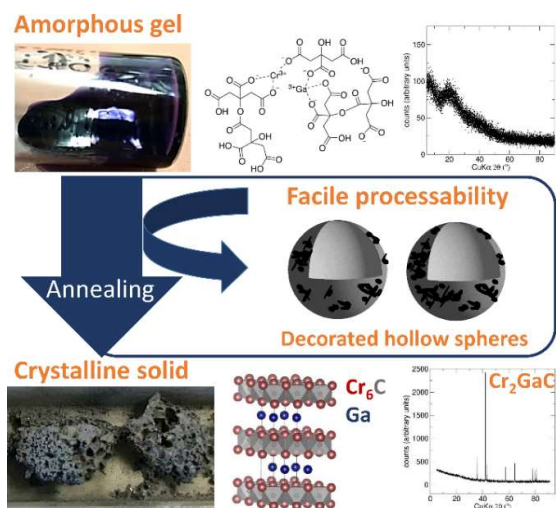
Figure 1: Schematic showing the transformation of the amorphous gel into a crystalline MAX phase solid by means of photographs (upper and lower left) and X-ray powder diffraction data (upper and lower right). The sol-gel approach allows for facile processability of the precursor gel resulting in Cr_2GaC-decorated hollow carbon spheres.
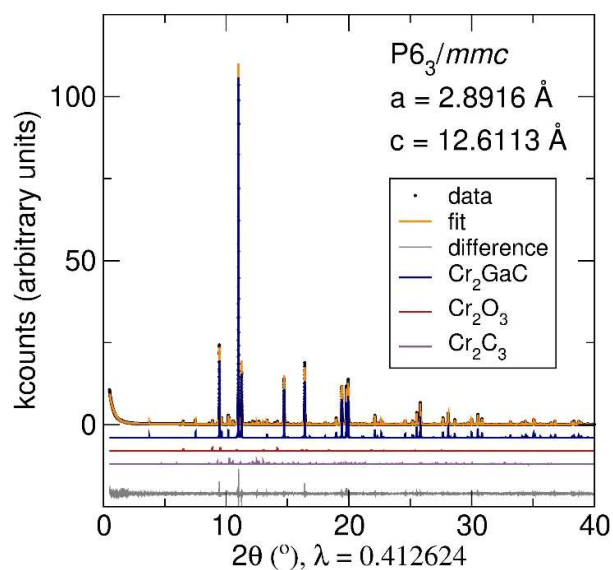

Figure 2: (a) Rietveld refinement (orange) and difference curve (grey) of the high-resolution synchrotron based X-ray powder diffraction data (black) of the final product. The main phase is the MAX phase Cr_2GaC (dark blue), Cr_2O_3 (dark red) and Cr_3C_2 (purple) can be identified as minor side phases.

In earlier works, we have developed a microwave heating method to prepare Cr- and V based MAX phases.[24–26] Cr_2GaC is one of the MAX family members that were initially synthesized and structurally characterized as H-phases in the early 1960s. The typical bulk/powder synthesis involves reacting metal precursors in evacuated quartz ampoules at around 1000 °C for multiple days.[27,28] Due to the difficulties to mix Ga with the other elemental precursors, a slightly different route was used in the case of Mn-doped Cr_2GaC where Ga pellets were placed on top of the powder mixture. This setup was heated at 975 °C for 24h.[29] Another approach is based on the carbothermal reduction of chromium oxide that enables the synthesis of Cr_2GaC (and M_2GeC with M = V, Cr) starting from Cr_2O_3 and Ga (Ge and V_2O_5, respectively).[30]

Although a large variety of possible synthesis pathways exist, a solution based method involving molecular precursors for the synthesis of MAX phases has not been developed yet. However, solution-processable precursors have the potential to be highly scalable, to be deposited by spin, spray, or dip coating, painted or printed, or fabricated in a variety of ways. Here, we report on the sol-gel based synthesis of MAX phase Cr_2GaC including elucidation of the formation mechanism by thermoanalysis. We further demonstrate the facile processability by preparing hollow carbon microspheres that are decorated with Cr_2GaC. The structure and morphology of the resulting materials are characterized by powder diffraction and electron microscopy and their magnetic properties are presented.

Synthesis and characterization

For a typical synthesis, the nitrate precursors $Cr(NO_3)_3*9H_2O$ (Honeywell, 98%) and $Ga(NO_3)_3*xH_2O$ (ChemPUR, 99,9%) and citric acid (Alfa Aesar, 99,5%) were weighed in air and dissolved in a minimal amount of DI-water (usually 10 ml).

The combination of nitrate (oxidizer) and citric acid (fuel) make this reaction a version of the solution combustion synthesis[10] that is a variation of a general sol-gel process. Consequently, a large variability of the reactions that take place exists, e.g. by using a different type of fuel.[31] In our case, we typically used a ratio of 2:1 for Cr:Ga ($Cr(NO_3)_3*9H_2O$: 2.695 mmol = 1.0784 g, $Ga(NO_3)_3*xH_2O$: 1.3475 mmol = 0.5398 g) and 9 equiv. of citric acid (0.012 mol = 2.33 g). After mixing the precursor compounds with water using a magnetic stir bar inside a beaker, the homogenous solution was heated to 70 °C – 80 °C on a heating plate until a viscous liquid was obtained. The gel was then transferred into a Al_2O_3 crucible in which the heat treatment was conducted. During the annealing process under flowing Ar (99.999%), the temperature was increased with a rate of 2 °C/min up to 900 °C using a horizontal tube furnace (Carbolite). The final temperature was held for five hours before cooling down to room temperature. In order to investigate the reaction process in more details, different samples were heated at temperatures between 600 °C and 900 °C for 5h. The general process along with photographs of the precursor gel and final product are shown in Fig. 1. Please note that X-ray powder diffraction data are intended to show the clear difference in crystallinity between the precursor gel and the product. A thorough investigation of the data follows in Fig. 2. An additional SEM image of the as-prepared material further shows its porous structure (Fig. SI-1). The formation mechanism was elucidated by thermal analysis coupled with mass spectrometry. Details can be found in the Supplementary Information. We also investigated the influence of an even higher excess in citric acid in the precursor mixture (20 equiv. of citric acid, details see SI) on the final product. This sample was used for the magnetic measurements.

For the synthesis of the decorated hollow microspheres, a sol-gel-impregnation process was established. It is based on the
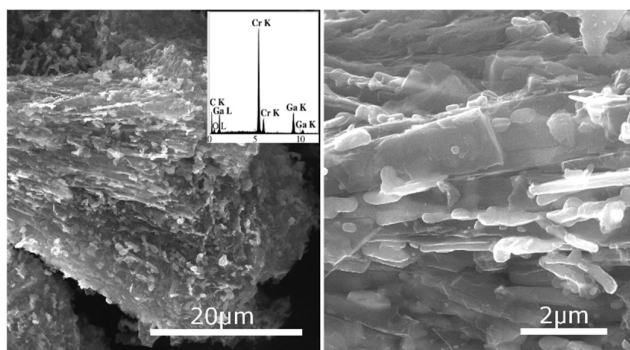
Figure 3: Electron micrographs showing the morphology of Cr$_2$GaC MAX phase particles.

above described sol-gel formation in aqueous solution, except that the water evaporation during gelation was interrupted after a slightly viscous sol was formed. After cooling, 200 mg Expancel (AkzoNobel, 921 WE 40 d24) was added to the sol and the reaction mixture was stirred for several minutes, followed by the separation of the residual sol. The impregnated Expancel was spread on a watch glass to avoid greater agglomeration and was dried at ambient conditions. Annealing was conducted in glassy carbon crucibles under an argon atmosphere forming partially agglomerated hollow spheres. Samples were investigated by X-ray powder diffraction, electron microscopy and magnetometry measurements.

Results and discussion

Structure and microstructure of Cr$_2$GaC

The final product was structurally investigated in detail by high resolution synchrotron X-ray powder diffraction data (Fig. 2) obtained at beamline 11BM (Advanced Photon Source (APS), Argonne National Laboratory). The data were refined using TOPAS Academic.[32] For the main phase Cr$_2$GaC, the structural model with space group $P6_3/mmc$ (as originally reported by Jeitschko et al.[27]) was fitted (orange line in Fig. 2) to the powder diffraction data (black dots in Fig. 2). The resulting refined unit cell parameters of a = 2.89161(0) Å and c = 12.61133(2) Å match those reported in the literature of a = 2.88(6) Å and c = 12.61(6) Å[27] very well. The side phases   could be identified as Cr$_2$O$_3$ and Cr$_3$C$_2$ and were also taken into account for the Rietveld refinement (Cr$_2$O$_3$: dark red line in Fig. 2, ~4.5 wt%, Cr$_3$C$_2$: violet line in Fig. 2, ~5 wt%). The higher background at very low angles is the result of amorphous carbon that remains in the final product after annealing at 900 °C under argon atmosphere. Laboratory-scale X-ray powder diffraction data were obtained for the sample prepared with a larger excess of citric acid (SI-2). The purity of the MAX phase product seems to be improved since no peaks of side phases could be identified. However, due to the higher amount of amorphous carbon in the product and the lower quality of the data, small amounts of side phases could still be present. The high amount of amorphous carbon can cause troubles with data acquisition and evaluation (especially for electron microscopy), thus the latter sample was only used for the magnetometry measurements.
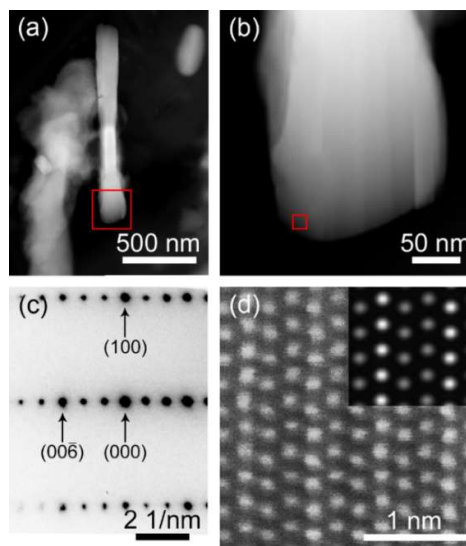

Figure 4: (a) Overview HAADF-STEM image of the analyzed needle-like structure. (b) high-resolution HAADF-STEM image of the section indicated with a red box. (c) SAED pattern of the same nanoparticle in [010] orientation. (d) Experimental HAADF-STEM image taken along the [010] zone axis of the region marked in (b), inset showing the QSTEM image simulation for the same orientation.

Electron micrographs (Fig. 3) show the microstructure of the ground crystalline product as obtained after the annealing step. Fragments of different sizes can be found whereas most of them exhibit an overall plate or rod-like and anisotropic morphology, as can be seen in Fig. 3 (left). EDX analysis (inset in Fig. 3) confirms the presence of the elements Cr, Ga and C (oxygen is also detected that stems from the Cr$_2$O$_3$ side phase).

The morphology differs from material obtained by classical high-temperature solid-state reactions, however, the layered structure is still visible (Fig. 3). On a more local scale, anisotropic and needle-like particles can be observed using transmission electron microscopy (Fig. 4 (a+b), Fig. SI-4). Analysis of a particle with a length and width of roughly 1600 nm and 200 nm, respectively, verifies the MAX phase structure by selected area electron diffraction (SAED) and high resolution high angle annular dark field (HAADF) imaging (Fig. 4 (c+d)). Additional image simulation along the [010] zone axis confirms the MAX phase (inset Fig. 4 (d)). Energy dispersive X-ray spectroscopy (EDS) further supports the presence of all expected elements in the particle (Fig. SI-5).

Anisotropic grain growth was also observed in Ti$_3$SiC$_2$ prepared by reactive hot isostatic pressing.[33] Moreover, anisotropic structures are also observed in other materials, such as different oxides, that were prepared by a solution combustion reaction.[10] While the formation of spherical particles is more common, plate- and rod-like particles can also be obtained. Varma et al. conclude in their review article that the morphology depends on the mechanism of structure formation, however, also point out that this process is not understood completely in the case of the anisotropic structure formation. They further summarize that the formation of rod-like crystals "likely grow by a gas – liquid – solid mechanism, typical for such crystals." In our case, there is indeed a large amount of different gases that can be involved in such processes (see Fig. 5(b)).
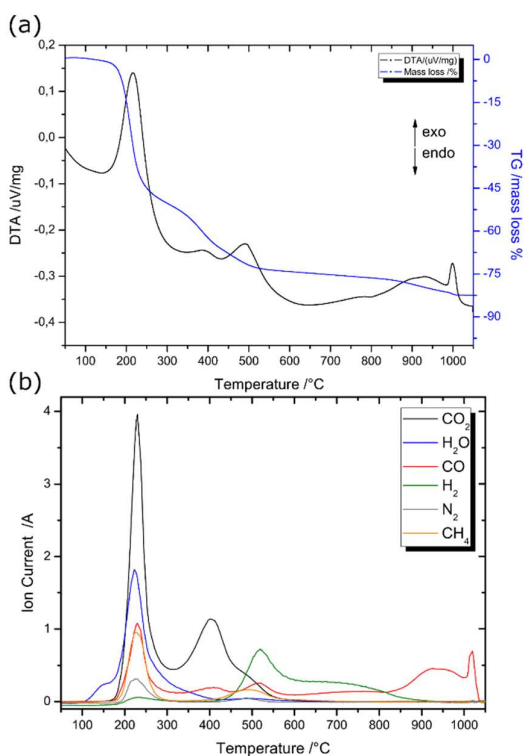
Figure 5: Simultaneous thermal analysis (DTA/TG) combined with on-line mass spectrometry of fully dried gel from room temperature to 1050 °C with a heating rate of 10 °C/min in flowing Ar (a) heat effects and mass changes and (b) analyzed pyrolysis and reaction products during formation of the MAX phase.
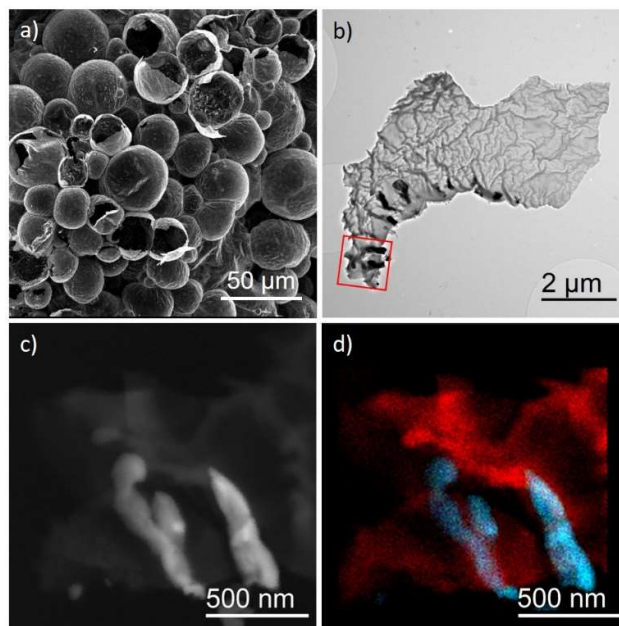

Figure 6: a) SEM overview of hollow microspheres. (b) BF-STEM overview of a fragment of a sphere. (c) Z-contrast (HAADF) STEM image of the marked region in (b), two phases with differing average Z number can be differentiated. (d) RGB coded (R-C_{Ka}, G-Ga_{Ka}, B-Cr_{Ka}) EDS map of the same region, a Ga and Cr rich phase and the C-rich wall can be observed.

Formation mechanism

Ex-situ X-ray powder diffraction data show the transformation of the amorphous gel into the crystalline MAX phase (Fig. SI-6). After heating at 600 °C and 700 °C for 5h, respectively, no peaks or only low intensity peaks are observed, respectively. After heating at 800 °C for 5h, peaks of Cr_2O_3 and MAX phase Cr_2GaC are found. Upon heating at 900 °C for 5h, a nearly single-phase compound was obtained.

The reaction mechanism was also investigated in detail by simultaneous thermal analysis combining differential thermal analysis (DTA) with thermogravimetry (TG) coupled with mass spectrometry (Fig. 5). Upon heating (uncertainty in temperature is ±5 °C), the dried gel – the fuel (citric acid) and the oxidizer (nitrates) – initially decomposes exothermally starting at ~150 °C into smaller fragments releasing gaseous CO_2, H_2O, CO, CH_4, N_2 and H_2.[10] Interestingly, the nitrate precursors are fully reduced to elemental N_2 by the excess carbon since no NO_x fragments are detected. The carboxylate complexes that bind the metal ions subsequently decompose around 300 °C resulting in the release of gaseous CO_2 and the formation of amorphous chromium and gallium oxide (Me = Cr, Ga):

$$Me^{3+} - (RCOO^-)_3 \xrightarrow{\Delta} Me_xO_y + C + CO_z \uparrow \quad (1)$$

Starting at 850 °C, the metal oxides are carbothermally reduced by elemental carbon releasing CO and subsequently react with excess carbon to form the final carbide phase at approximately 1000 °C (Me^1 = Cr, Me^2 = Ga):

$$2Me_x^1O_y + Me_x^2O_y + C \xrightarrow{\Delta} Me_{\frac{1}{2}}^1Me^2C + CO_y \uparrow \quad (2)$$
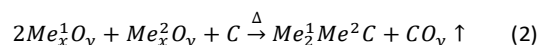
In the thermal analysis experiments, the formation temperature of the MAX phase appears slightly higher than in the furnace experiments. This can be explained by the higher heating rate and dynamic nature of the heating process during thermal analysis in contrast to the much slower heating and the 5 h isothermal section at 900 °C during the synthesis of the final product in the tube furnace. Additionally, no identical atmospheric conditions could be adjusted in the different experiments, which play a crucial role in reduction reactions. In thermal analysis and during synthesis in the tube furnace, a constant Ar flow of 50 ml/min and 333 ml/min was provided, respectively.

Processability of Cr_2GaC

Our sol-gel approach involves a wet chemical treatment prior to the annealing step where the amorphous precursors are transformed into the final MAX phase. In contrast to typical solid-state reactions, this initial wet chemical process is highly flexible allowing easy processability of the precursor mixture. Here, we demonstrate this facile route by preparing hollow carbon microspheres that are decorated with the Cr_2GaC MAX
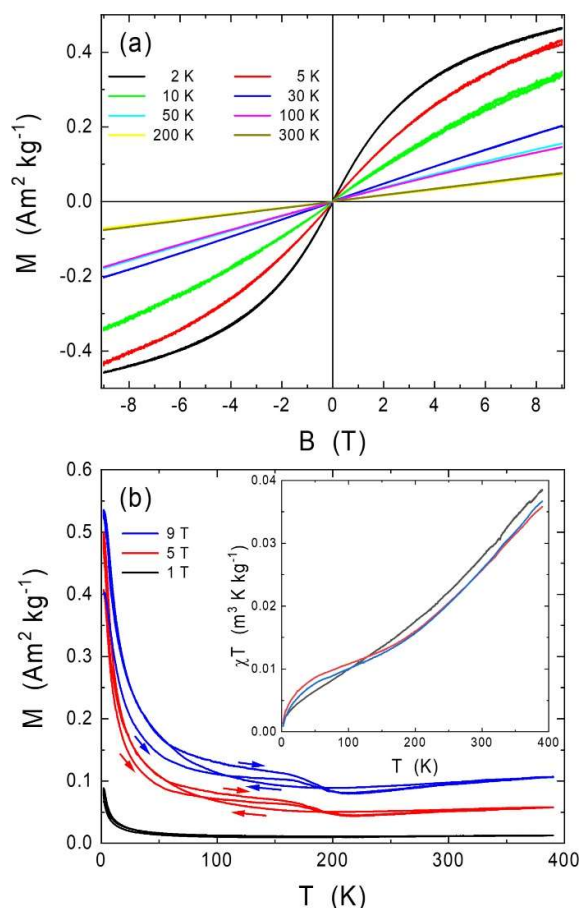
phase. Expancel hollow microspheres have been used before in a different study where we prepared phosphor microspheres.[34]

Figure 7: (a) Magnetization as function of magnetic induction as various temperatures. (b) ZFC/FC/FW curves at B = 1 T, 5 T, and 9 T. The arrows indicate the scan directions with temperature. The inset shows the product of magnetic susceptibility χ and temperature T as function of temperature for the FC scans.

They were added during the gel-forming step and transformed into a carbon matrix during annealing of the precursor mixture. X-ray powder diffraction data confirm the presence of crystalline Cr_2GaC (Fig. SI-7). The resulting refined unit cell parameters of a = 2.89373(2) Å and c = 12.6155(2) Å match those of the sol-gel derived particles as well as those reported in the literature.[27] The large background at low angles is ascribed to amorphous carbon (microsphere template). A minimal amount of chromium carbide as a side phases is found, similar to the initially prepared Cr_2GaC MAX phase if a large excess of citric acid (carbon source) is used.

The overall morphology of the hollow microspheres can be observed in an overview electron micrograph (Fig. 6 (a)). The carbon hollow spheres have formed in sizes between roughly 25 and 45 μm in diameter which mirrors the shape and size of the initial Expancel template. Some spheres are broken showing their hollow nature as well as relatively thin walls (approximately 100-300 nm). A fragment of one of the microspheres was investigated in further detail by transmission electron microscopy techniques. The Z-contrast (HAADF) STEM image shows two different phases with differing average Z

number (Fig. 6 (b+c)). Element specific analysis confirms the presence of two different phases: amorphous carbon of the wall of the microspheres (shown in red in Fig. 6 (d)) and a Cr and Ga-rich phase, Cr_2GaC according to X-ray powder diffraction (Fig. SI-6), shown in light blue (result of overlaying green and blue in Fig. 6 (d)). The anisotropic shape of the particles can also be observed when deposited on the surface of the hollow carbon microspheres.

Magnetic properties

The magnetic response of the sol-gel prepared Cr_2GaC samples are inspected by vibrating sample magnetometry (VSM) in magnetic induction of B = ± 9 T and temperatures T = 2-390 K. Fig. 7 (a) presents magnetization curves as functions of induction B. We observe in the temperature interval 2-390 K a paramagnetic response as reported earlier for Cr_2GaC[35] and Cr_2AlC.[36] The shape of the magnetization curve at T = 2 K shows the characteristics of a Langevin paramagnet which, however, does not saturate at 2 K and 9 T and might be superimposed by an additional Pauli paramagnetic contribution. The magnetization M (2 K, 9 T) = 0.465 Am^2kg^{-1} translates into a magnetic moment 0.015 μ_B per formula unit. This low moment per formula unit is in line with previous reports of 0.05 μ_B per Cr atom for Cr_2AlC, 0.02 μ_B per Cr atom for Cr_2GeC[37] and 0.005 μ_B per formula unit at T = 2 K at B = 6 T for Cr_2GaC.[38] When the temperature is increased, the curvature changes to a strictly linear response above T = 30 K. We tested further whether the scans at various temperatures merge to a master curve when plotted as function of the ratio B over T (Fig. SI-7). It is obvious that the zero-field susceptibility (slope at B = 0) increases with rising temperature in these units and thus the sample does not obey the Curie law, even after subtraction of the temperature independent Pauli paramagnetic contribution. Thus, additional components with magnetic correlations are present in the sample.

Temperature-dependent zero-field cooled, field-cooled and field warming (ZFC/FC/FW) curves may allow to discriminate between the different components summing up to the measured data. Fig. 7 (b) shows the curves for B = 1 T, 5 T and 9 T, respectively. The overall shape suggests a mixture of Langevin (T^{-1}-dependence) and Pauli (constant) paramagnetism as observed before for various MAX phases like $(V/Mn)_2AlC$[25] or Cr_2GaC.[38] On top, however, there is a small, but significant splitting of ZFC/FC/FW curves indicating correlations of the magnetic moments in the sample. Note that the scan for B = 1 T also exhibits such behaviour when rescaling. It is unlikely that these correlations originate from Cr_2GaC, but rather from small amounts of side phases, which do not show up in the X-ray diffraction data. The sample under investigation is essentially phase pure (See Fig. SI-2) and thus we speculate on some oxidation of Cr in the sol-gel sample exhibiting a huge surface area with respect to samples prepared by solid-state reactions.[28] Cr_2O_3 is antiferromagnetic with T_N = 308 K in the bulk and shows reduced ordering temperatures and superparamagnetism in nanoparticles.[39] We ascribe the splitting in the ZFC/FC/FW curves to such nanoscale effects. Nonetheless, at high temperatures the measurement is clearly

dominated by a temperature-independent contribution stemming from the Cr_2GaC MAX phase which is evaluated next. Further analysis of the FC curves at T = 390 K in Fig. 7 (b) yields a strictly linear dependence of the magnetic susceptibility χ = $1.17 \cdot 10^{-2}$ Am^2 $kg^{-1}T^{-1}$ translating to $1.47 \cdot 10^{-8}$ m^3 kg^{-1} ($2.73 \cdot 10^{-9}$ m^3 mol^{-1}) at T = 390 K. Plotting $\chi \cdot T$ as function of temperature in the inset of Fig. 7 (b) in principle allows for the discrimination of Langevin and Pauli paramagnet contributions to the measured signal. Above about T = 250 K we indeed observe a linear dependence for all applied fields from which the Pauli contribution is calculated to χ_P = $(3.46 \pm 0.17) \cdot 10^{-9}$ m^3 mol^{-1}. From χ_P the density of states at the Fermi level can be calculated to $D(E_F)$ = $\chi_P \cdot (\mu_0 \mu_B^2) - 1$ = (8.49 ± 0.42) eV^{-1} per formula unit with μ_0 the vacuum permeability and μ_B Bohr's magneton. Note that this results stems from experimental data far off the region of the magnetic correlations. The present result is fully in line with previous reports on the Fermi energy of Cr_2GaC of 8.6 eV^{-1} per formula unit reflecting the success of the sol-gel preparation process.[40]

Extrapolation of the linear slope to the ordinate yields the contribution of the Langevin paramagnetism in solely paramagnetic samples. Here, however, such analysis is not possible due to the masking magnetic correlations. The investigations of the Cr_2GaC MAX phase on the hollow carbon sphere has also been undertaken. In this case the overall magnetic response is similar, but the diamagnetic contribution of the carbon shells additionally complicates the analysis.

Conclusions

We have successfully developed a new sol-gel based – solution combustion – synthesis method for the preparation of MAX phase Cr_2GaC. The most significant advantage of this initially wet chemical technique is the enhanced processability of the precursor mixture – here demonstrated by the preparation of hollow carbon microspheres that are decorated with MAX phase particles. Synchrotron X-ray powder diffraction data reveal highly crystalline Cr_2GaC with small amounts of side phases Cr_2O_3 and Cr_3C_2. The amount of oxide can further be reduced by increasing the excess of citric acid in the precursor mixture. Although the intimately mixed precursor gel is heated at relatively high temperatures in order to obtain crystalline Cr_2GaC, the morphology differs from conventionally prepared bulk MAX phases. The product crystallizes in the form of agglomerated anisotropic particles (length and width of the needle-shaped particles vary in the sample). Detailed thermal analysis elucidates the formation process that includes the carbothermal reduction of amorphous gallium and chromium oxides followed by crystallization of the target MAX phase. The samples are essentially Pauli paramagnets with a density of states at the Fermi level of 8.5 eV^{-1} per formula unit while additional low temperature splitting of the temperature-dependent magnetization is ascribed to the side phases.

References

1   L. L. Hench and J. K. West, *Chem. Rev.*, 1990, **90**, 33–72.
2   R. Roy, *J. Am. Ceram. Soc.*, 1956, **39**, 145–146.
3   R. Roy, *J. Am. Ceram. Soc. Notes*, 1969, **52**, 344.
4   P. J. Flory, *Faraday Discuss. Chem. Soc.*, 1974, **57**, 7–18.
5   A. E. Danks, S. R. Hall and Z. Schnepp, *Mater. Horizons*, 2016, **3**, 91–112.
6   C. Giordano, A. Kraupner, S. C. Wimbush and M. Antonietti, *Small*, 2010, **6**, 1859–1862.
7   C. Giordano, C. Erpen, W. Yao, B. Milke and M. Antonietti, *Chem. Mater.*, 2009, **21**, 5136–5144.
8   A. M. Stux, C. Laberty-Robert and K. E. Swider-Lyons, *J. Solid State Chem.*, 2008, **181**, 2741–2747.
9   L. Zhao, K. Fang, D. Jiang, D. Li and Y. Sun, *Catal. Today*, 2010, **158**, 490–495.
10   A. Varma, A. S. Mukasyan, A. S. Rogachev and K. V. Manukyan, *Chem. Rev.*, 2016, **116**, 14493–14586.
11   W. Jeitschko, *Monatsh. Chem. Verw. Teile Anderer Wiss.*, 1963, **94**, 672–676.
12   M. W. Barsoum, *Prog. Solid State Chem.*, 2000, **28**, 201–281.
13   M. W. Barsoum, *MAX phases: Properties of Machinable Carbides and Nitrides*, 2013.
14   M. Radovic and M. W. Barsoum, *Am. Ceram. Soc. Bull.*, 2013, **92**, 20–27.
15   A. S. Ingason, M. Dahlqvist and J. Rosén, *J. Phys. Condens. Matter*, 2016, **28**, 433003.
16   M. Naguib, M. Kurtoglu, V. Presser, J. Lu, J. Niu, M. Heon, L. Hultman, Y. Gogotsi and M. W. Barsoum, *Adv. Mater.*, 2011, **23**, 4248–53.
17   B. Anasori, M. R. Lukatskaya and Y. Gogotsi, *Nat. Rev. Mater.*, 2017, **2**, 16098.
18   J. C. Schuster, H. Nowotny and C. Vaccaro, *J. Solid State Chem.*, 1980, **32**, 213–219.
19   S. Arunajatesan and A. H. Carim, *J. Am. Ceram. Soc.*, 1995, **78**, 667–672.

20   I. M. Low, Ed., *Advances in Science and Technology of Mn+1AXn Phases*, Woodhead Publishing, 2012.

21   A. Julian-Jankowiak and P. Sallot, *Ceram. Int.*, 2018, **44**, 16314–16324.

22   E. Salahi, M. Akhlaghi, S. A. Tayebifard, G. Schmidt and M. Shahedi Asl, *Ceram. Int.*, 2018, **44**, 9671–9678.

23   E. A. Levashov, Y. S. Pogozhev, D. V. Shtansky and M. I. Petrzhik, *Russ. J. Non-Ferrous Met.*, 2009, **50**, 151–159.

24   C. M. Hamm, J. D. Bocarsly, G. Seward, U. I. Kramm and C. S. Birkel, *J. Mater. Chem. C*, 2017, **5**, 5700–5708.

25   C. M. Hamm, M. Dürrschnabel, L. Molina-Luna, R. Salikhov, D. Spoddig, M. Farle, U. Wiedwald and C. S. Birkel, *Mater. Chem. Front.*, 2018, **2**, 483–490.

26   C. M. Hamm, T. Schäfer, H. Zhang and C. S. Birkel, *Zeitschrift für Anorg. und Allg. Chemie*, 2016, **642**, 1397–1401.

27   W. Jeitschko, *Monatsh. Chem. Verw. Teile Anderer Wiss.*, 1963, **94**, 844–850.

28   S. Lin, P. Tong, B. S. Wang, Y. N. Huang, W. J. Lu, D. F. Shao, B. C. Zhao, W. H. Song and Y. P. Sun, *J. Appl. Phys.*, 2013, **113**, 53502.

29   A. Mockute, J. Lu, E. J. Moon, M. Yan, B. Anasori, S. J. May, M. W. Barsoum and J. Rosen, *Mater. Res. Lett.*, 2014, **3**, 16–22.

30   D. T. Cuskelly and E. H. Kisi, *J. Am. Ceram. Soc.*, 2016, **99**, 1137–1140.

31   K. V. Manukyan, A. Cross, S. Roslyakov, S. Rouvimov, A. S. Rogachev, E. E. Wolf and A. S. Mukasyan, *J. Phys. Chem. C*, 2013, **117**, 24417–24427.

32   A. Coelho, 2007.

33   T. El-Raghy, M. W. Barsoum, A. Zavaliangos and R. S. Kalidindi, *J. Am. Ceram. Soc.*, 1999, **82**, 2855–2860.

34   L. Bischoff, M. Stephan, C. S. Birkel, C. F. Litterscheid, A. Dreizler and B. Albert, *Sci. Rep.*, 2018, **8**, 602.

35   Z. Liu, T. Waki, Y. Tabata, K. Yuge, H. Nakamura and I. Watanabe, *Phys. Rev. B*, 2013, **88**, 134401.

36   R. Boucher, O. Berger and C. Leyens, *Surf. Eng.*, 2016, **32**, 172–177.

37   M. Jaouen, M. Bugnet, N. Jaouen, P. Ohresser, V. Mauchamp, T. Cabioc'h and A. Rogalev, *J. Phys. Condens. Matter*, 2014, **26**, 176002.

38   Z. Liu, T. Waki, Y. Tabata and H. Nakamura, *Phys. Rev. B*, 2014, **89**, 54435.

39   D. Tobia, E. L. Winkler, R. D. Zysler, M. Granada and H. E. Troiani, *J. Alloys Compd.*, 2010, **495**, 520–523.

40   Z. Liu, K. Takao, T. Waki, Y. Tabata and H. Nakamura, *J. Phys. Conf. Ser.*, 2017, **868**, 12016.
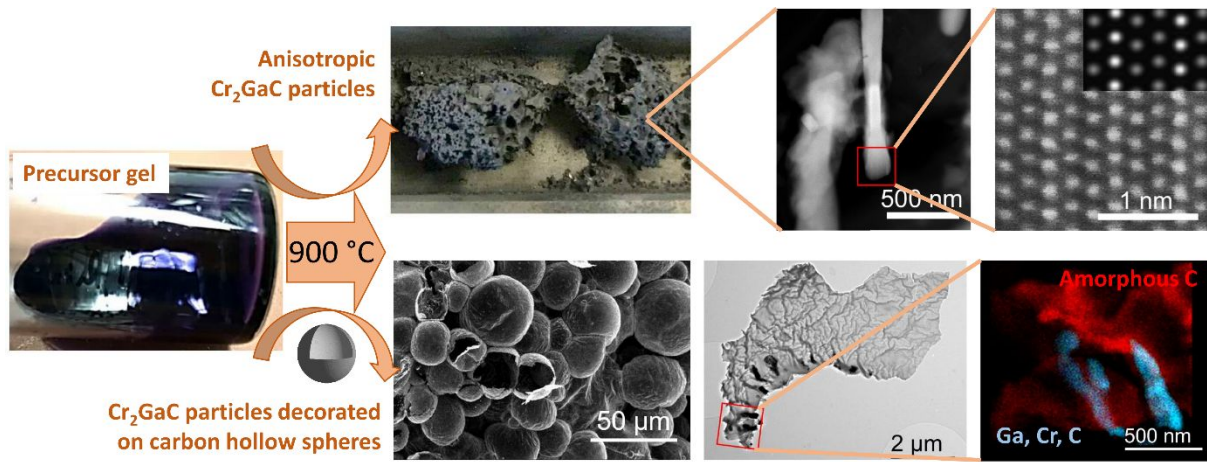
New and facile wet chemistry based synthesis method for the preparation and processing of MAX phase Cr_2GaC